Magnetism as indirect tool for carbon content assessment in nickel nanoparticles

Y. Oumellal, Y. Magnin, A. Martínez de Yuso, J. M. Aguiar Hualde, H. Amara, V. Paul-Boncour, C. Matei Ghimbeu, A. Malouche, C. Bichara, R. Pellenq, and C. Zlotea

Citation: Journal of Applied Physics **122**, 213902 (2017);
View online: https://doi.org/10.1063/1.5006138
View Table of Contents: http://aip.scitation.org/toc/jap/122/21
Published by the American Institute of Physics

JOURNAL OF APPLIED PHYSICS **122**, 213902 (2017)

Magnetism as indirect tool for carbon content assessment in nickel nanoparticles

Y. Oumellal,[1] Y. Magnin,[2,3] A. Martínez de Yuso,[4] J. M. Aguiar Hualde,[5] H. Amara,[5] V. Paul-Boncour,[1] C. Matei Ghimbeu,[4] A. Malouche,[1] C. Bichara,[2] R. Pellenq,[3] and C. Zlotea[1,a)]

[1]*Université Paris Est, Institut de Chimie et des Matériaux Paris-Est (UMR7182), CNRS, UPEC, 2-8 rue Henri Dunant, 94320 Thiais, France*
[2]*Aix Marseille Université, CNRS, CINAM, Campus de Luminy, 13288 Marseille, France*
[3]*MultiScale Material Science for Energy and Environment, Massachusetts Institute of Technology-CNRS Joint Laboratory at Massachusetts Institute of Technology, Cambridge, Massachusetts 02139, USA*
[4]*Université de Strasbourg, Université de Haute-Alsace, Institut de Science des Matériaux de Mulhouse (UMR 7361), CNRS, 15 rue Jean Starcky, 68057 Mulhouse, France*
[5]*Laboratoire d'Etude des Microstructures (UMR 104), CNRS-ONERA, 29 avenue de la Division Leclerc, 92322 Chatillon, France*

(Received 22 September 2017; accepted 11 November 2017; published online 5 December 2017)

We report a combined experimental and theoretical study to ascertain carbon solubility in nickel nanoparticles embedded into a carbon matrix *via* the one-pot method. This original approach is based on the experimental characterization of the magnetic properties of Ni at room temperature and Monte Carlo simulations used to calculate the magnetization as a function of C content in Ni nanoparticles. Other commonly used experimental methods fail to accurately determine the chemical analysis of these types of nanoparticles. Thus, we could assess the C content within Ni nanoparticles and it decreases from 8 to around 4 at. % with increasing temperature during the synthesis. This behavior could be related to the catalytic transformation of dissolved C in the Ni particles into graphite layers surrounding the particles at high temperature. The proposed approach is original and easy to implement experimentally since only magnetization measurements at room temperature are needed. Moreover, it can be extended to other types of magnetic nanoparticles dissolving carbon. *Published by AIP Publishing.* https://doi.org/10.1063/1.5006138

I. INTRODUCTION

Nickel-based materials are widely used in many manufactured products and have significantly contributed to the progress of our present-day society. Pure Ni has good mechanical properties and resistance to a range of corrosive media together with good thermal and electrical properties. Consequently, the magnetic properties of both bulk and nanosized Ni materials are very well documented.[1–5] Besides magnetism, Ni is a well known catalyst for the growth of carbon nanotubes (CNTs), where metal nanoparticles (NPs) are required to enable hydrocarbon decomposition at a temperature lower than the spontaneous decomposition temperature of the hydrocarbons.[6] Indeed, efficient catalysts to grow CNTs lie in the 1–10 nm diameter range and are reported to display non-zero, but limited carbon solubility in the bulk solid.[7,8] This is typically the case for Ni, where the solubility limit is around 5%–6% according to the bulk phase diagram.[9] At the nanoscale, C incorporation in the catalyst NPs, together with its size reduction, modifies its physical and chemical states as compared to the bulk alloy. Carbon rich phase diagrams of Ni-C nanoparticles have been calculated for system sizes up to about 3 nm, highlighting how C atoms can diffuse inside surface layers and induce a partial or complete melting.[10] In the context of CNT growth, it has been recently shown that the carbon content inside the NP favors the dewetting of the nanoparticles with respect to the sp^2 carbon wall, a necessary property to limit catalyst encapsulation and deactivation.[11,12]

In this context, the control of the size, shape, and chemical composition of Ni nanoparticles supported/embedded into porous carbon is of paramount importance for many types of applications. Among a large variety of synthetic methods, the soft-template route involving the co-assembly of phenolic resins and metal salt precursors in the presence of organic templates is a very convenient and fast method for the preparation of composite materials for a wide range of applications.[13–15] These composites contain (oxide or metallic) nanoparticles inserted into a porous carbon framework.

We have recently reported an easy and rapid one-pot microwave assisted soft-template synthesis method for the preparation of Pd-Ni nanoalloys confined in mesoporous carbon.[14] This approach allows the formation of mesoporous carbon and the growth of the particles at the same time, under short microwave irradiation (4 h) followed by thermal annealing at temperatures above 730 K. Despite the simple synthesis approach from the practical point of view, during this last step, several events occur. At low temperature (<523 K), the phenolic resin crosslink allows the formation of more a rigid structure and the metallic salts are decomposed usually to their oxide forms. At higher temperature (580–730 K), the decomposition of phenolic resin and template leads to the formation of a mesoporous carbon

[a)]Author to whom correspondence should be addressed: claudia.zlotea@icmpe.cnrs.fr

network.[16] For further increase of the temperature, oxygen functional groups are removed from the carbon network which become a good reduction medium for metal oxide particles to be reduced to their metallic form by the carboreduction process.[16–18]

Depending on the carbon framework structure, location/confinement of the particles in the carbon, the size, and the catalytic properties of the metallic particles, carbon graphitization around the particles occurs at a rather low temperature.[14,15] The graphitization mechanism of carbon in the presence of metallic nanoparticles has already been studied and it strongly depends on the metal type.[19,20] Two mechanisms are widely accepted to explain the carbon catalytic graphitization: (i) the dissolution-precipitation mechanism, where the amorphous carbon is first dissolved into the metal catalyst and then precipitates as graphitic carbon and (ii) the formation of metal carbides which further decompose at a certain temperature, forming graphitic carbon.[20]

For Ni particles, several studies showed a mechanism by dissolution-precipitation, however, the determination of the amount of carbon dissolved in the metallic particles is difficult to assess, and previous studies, to our knowledge, have not been reported so far.

In the present study, we report the magnetic properties of Ni confined into carbon composites prepared at different temperatures. We propose here an original approach based on the experimental characterization of the magnetic properties of Ni at room temperature and Monte Carlo simulations used to construct the magnetization isotherms as a function of carbon content in Ni. This is an elegant way to assess the C content of Ni nanoparticles, where other experimental techniques are not adapted for the chemical analysis of such carbon-based composites. As it concerns the link between magnetism of Ni-based nanoparticles and carbon nanostructures, this approach has been previously used as a quantification tool for the assessment of Ni-based catalyst residues in purified CNTs.[21]

II. EXPERIMENTAL PART

A. Synthesis

Mesoporous Ni@C composites were synthesized by the one-pot soft-template microwave assisted method.[14] In a typical synthesis, block copolymer Pluronic F127 (0.81 g) and phloroglucinol (0.41 g) were dissolved in 9 ml of ethanol absolute in a flat-bottomed flask. An adequate amount of $Ni(NO_3)_2{\cdot}6H_2O$ metallic salt solved in 1 ml of water, was added to this solution drop by drop to ensure a homogeneous mixture. After few minutes of mixing, 0.05 g of citric acid was added followed by the addition of glyoxal (0.405 ml). The resulting solution was stirred for 10 min and MW-irradiated using a CEM Discover set-up with a maximum irradiation power of 25 W. During the microwave treatment, the solvent is evaporated at 313 K for 3 h and a phenolic-resin gel is obtained which is further progressively heated up to 348 K (30 min) in order to better polymerize the material. Finally, the material was thermally treated at several temperatures from 773 to 973 K for 1 h under Ar flow with a heating rate of 2 K/min. The total final metal quantity was set to ~5 wt. % with respect to the carbon framework (which was ~0.4 g). The Ni@C composites will be further called Ni@C-*x*, where *x* stands for the synthesis temperature: 773, 798, 823, 848, 873, and 973 K.

B. Characterizations

The sample morphologies were evaluated by transmission electron microscopy (TEM) with a Jeol ARM-200F instrument working at 200 kV.

Thermo-gravimetric analysis (TGA) was used to determine the Ni content in the material by heating at 10 K/min up to 1073 K under air (METTLER-TOLEDO TGA 851e). The Ni quantity was calculated based on the NiO mass residue.

X-ray powder diffraction (XRD) data were collected with a Bruker D8 ADVANCE A25 in the Bragg-Brentano θ-θ geometry equipped with a rear graphite (002) monochromator (Cu $K_{\alpha 1,2}$) motorized divergence slits.

Magnetic characterizations were performed with the help of a MANICS-DSM8 magnetometer operating up to 1.8 T. The magnetization curves versus field were measured at 300 K. The magnetization values were calculated by taking into account the total mass of composites. The saturation magnetization (M_S) was estimated by the extrapolation of the linear part of the magnetization curve at zero field.

C. Tight-binding Hamiltonian and classical Heisenberg term

To describe the Ni-C system, we have developed a tight-binding (TB) model based on the recursion method to calculate the local density of electronic states on each site leading to a relatively fast scheme of order N.[22] This interatomic energy model is then implemented in a Monte Carlo computer simulation code, used to relax the structures. Simulations in the grand canonical (GC) ensemble have been already used to study the catalytic growth of carbon structures (graphene and CNTs) on Ni.[23,24] This TB potential includes all relevant physics for describing the structural properties of the Ni-C system, while remaining simple enough to allow simulation of real experimental situations with hundreds or even thousands of atoms. In this context, no magnetic term was included since, contrary to other systems (such as Fe,[25] Fe-C,[26] and CoPt[27]), the magnetic and structural effects are not coupled. This is particularly true in the presence of C, since the magnetic moment of Ni atoms decreases quickly with C addition.[28] To study the magnetic properties, we have to add a classical Heisenberg term to the TB Hamiltonian (H_{TB}) with a fixed spin, depending on the carbon fraction dissolved inside the metal

$$H_{xyz} = H_{TB} + \sum_{i<j} J_{ij}\zeta(n_c) S_i S_j. \quad (1)$$

For pure Ni, such an approach can be seen as an approximation since it is known that magnetism of Ni is a particular case presenting spin magnitude variation. A more sophisticated method, such as renormalized random-phase approximation, should be employed.[29] This difficulty is overcome in the presence of C atoms, where a model with fixed spins is

valid. Moreover, the aim of the present work is to develop a model, both simple and accurate, to undertake appropriate large scale simulations when dealing with NPs containing hundreds of atoms.

As a first step, the present model was checked to correctly reproduce magnetic properties in the bulk system. All parameters in Eq. (1) are adjusted from bulk Ni-C DFT calculations[30] as follows: $J = 50\,\text{meV}$[30] is the Ni-Ni magnetic coupling between a spin S located at site i and interacting with a nearest neighbor located at site j, $S = 0.3$ in order to fit T_C for pure Ni bulk, and $\zeta(x_C)$ is a function which decreases the spin coupling as a function of the local C coordination surrounding Ni sites. This function was fitted against finite temperature DFT calculations.[30] To calculate the magnetic moments at different temperatures ($50\,\text{K} < T < 900\,\text{K}$) and composition ranges ($0\,\text{at.}\,\% < x_C < 14\,\text{at.}\,\%$), we performed Monte Carlo (MC) simulations in the isothermal-isobaric (NPT) ensemble. For each temperature and carbon concentration, we relax the system during at least 10^6 Monte Carlo steps. One Monte Carlo step corresponds at least to one move of each atom of the system. Once equilibrium is reached, we first equilibrate spins over 2×10^6 steps with the Monte Carlo procedure and average the magnetization over 10^6 steps. We reproduce this procedure for 10^3 different stable configurations allowing a large magnetization statistic. As seen in Fig. 1, our results are in a good agreement with the experimental measurements of the Curie temperature as a function of the C concentration.[31] The present set of calculations, therefore, confirms that the magnetic description provided by our TB Hamiltonian coupled to a classical Heisenberg term is accurate. Therefore, it will be used to calculate the magnetic properties of Ni NPs containing different concentrations of C atoms.

To understand the dependence of magnetic properties of Ni systems on the carbon concentration, we perform density-functional theory (DFT) calculations on a supercell of Ni containing 216 atoms for a concentration of C varying from 0 to 33 at. %. In these structures, the C atoms are randomly distributed in octahedral sites of the fcc Ni since, it is well-known that C occupies interstitial positions due to its relatively small atomic size.[32,33] It should be noted that a concentration of 25 at. % corresponds to the Ni_3C structure, which has been the subject of scientific investigations due to its potential for industrial applications. As a result, the orthorhombic cementite-type structure of Ni_3C described by Fang *et al.*,[28] has been considered in the following: the first-principles code Quantum Espresso[34] employing the density functional theory (DFT) within the projector-augmented wave (PAW) method[35] was used for all calculations. The generalized gradient approximation (GGA)[36] was employed for the exchange and correlation energy terms, because the GGA describes spin-polarized transition metals and compounds better than the local-density approximation (LDA). Integrations over the Brillouin zone are based on a $2 \times 2 \times 2$ Monkhorst-Pack three-dimensional grid for 216 atom cells. Calculations were performed at zero pressure, i.e., the relaxation of the atoms and the shape of the simulation cell are considered using the conjugate gradient minimization scheme. The atomic positions were relaxed until the magnitude of the forces on all the atoms was smaller than 0.04 eV/Å. In the case of pure fcc Ni, the calculations showed a ferromagnetic ordering with a moment of about 0.65 μ_B per Ni, in agreement with previous calculations.[28,37] We also performed calculations for dilute C solution in Ni. For this purpose, a supercell containing 216 Ni atoms and one C atom was employed. The calculations showed that the addition of a C atom in an octahedral site of the *fcc* Ni lattice costs +0.42 eV/C close to the experimental and theoretical values.[33,38]

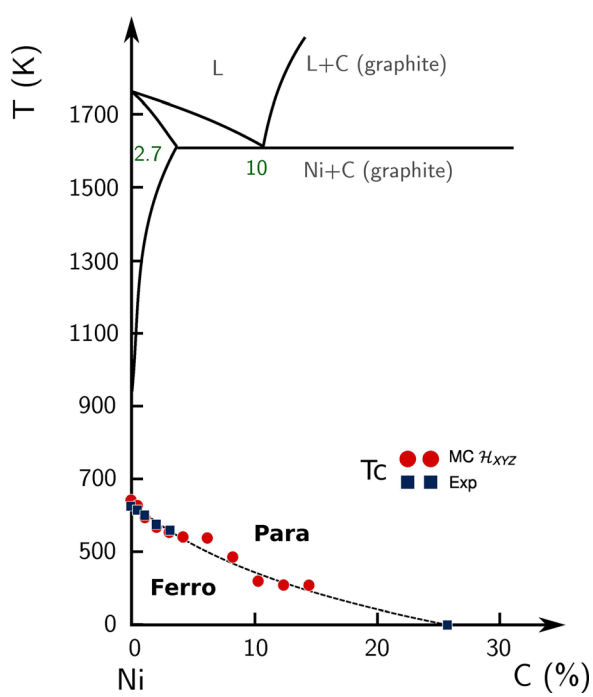

FIG. 1. Variation of Curie temperature determined experimentally (blue squares) and by MC simulations (red circles).

III. RESULTS AND DISCUSSIONS

A. Structure and microstructure of one-pot Ni@C-*x* composites

The one-pot synthetic method allows producing simultaneously dispersed metal nanoparticles and a mesoporous carbon matrix from a mixture of precursors by thermal annealing under inert gas at a certain temperature which depends on the nature of the precursors.[14,15,39] The optimization of the one-pot method produces well distributed nanoparticles within the carbon spaces with controlled textural properties and nanoparticle size.[15]

The structural analysis of one-pot Ni@C-x composites ($x = 773$, 798, 823, 848, 873, and 973 K) was carried out by XRD (Fig. 2). All composites show three main diffraction peaks from cubic Ni (*fcc* type structure) proving the reduction of the Ni precursor and formation of metallic Ni nanoparticles, irrespective of the temperature. The lattice parameter of the *fcc* structure for all composites is $a = 3.530(2)$ Å, which is slightly larger than 3.524 Å for the pure bulk metal.

The carbon host is XRD amorphous since the diffraction peaks at 26° corresponding to the (002) planes of graphitic carbon could not be observed. This is in a good agreement with

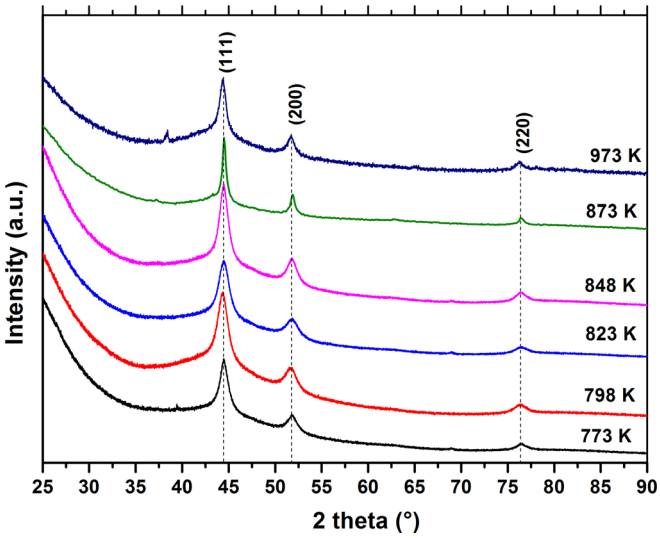

FIG. 2. XRD patterns of Ni@C-x composites ($x = 773$, 798, 823, 848, 873, and 973 K). The Miller indices corresponding to the *fcc* Ni phase are marked.

the Raman spectra proving rather amorphous carbon materials (Fig. SI-1, supplementary material). Typically D and G bands are seen, and their evolution with temperature indicates only slight improvements in the structural ordering.[18,40]

Microstructural analyses of Ni@C-x composites were carried out by TEM. Figure 3 shows typical bright field TEM images of all Ni@C-x composites. Ni nanoparticles are well distributed within the carbon host. From statistical analysis of several TEM images, particle size histograms could be determined (Fig. SI-2, supplementary material) and the average particle sizes are listed in Table I. The particle size increases with the thermal annealing temperature from 5.2 to 12.4 nm for 773 K to 973 K, respectively. This can be explained by temperature induced sintering and growth of Ni nanoparticles, in agreement with previous reports using one-pot methods.[15,41]

Carbon combustion experiments have been carried out by TGA in order to determine the Ni content in the Ni@C-x composites (Table I) under the hypothesis that the final combustion product is NiO. The Ni compositions in all Ni@C-x composites vary between 4.6 and 5.7 wt. %, in good agreement with the nominal metal amount set in the synthesis procedure. Along with the Ni quantity, TGA experiments also provide useful information related to the carbon matrix. Figure SI-3 (supplementary material) shows the TGA and related derivative curves for all composites. The combustion temperature [maximum of the derivative curves in Fig. SI-3 (supplementary material) given in Table I] generally

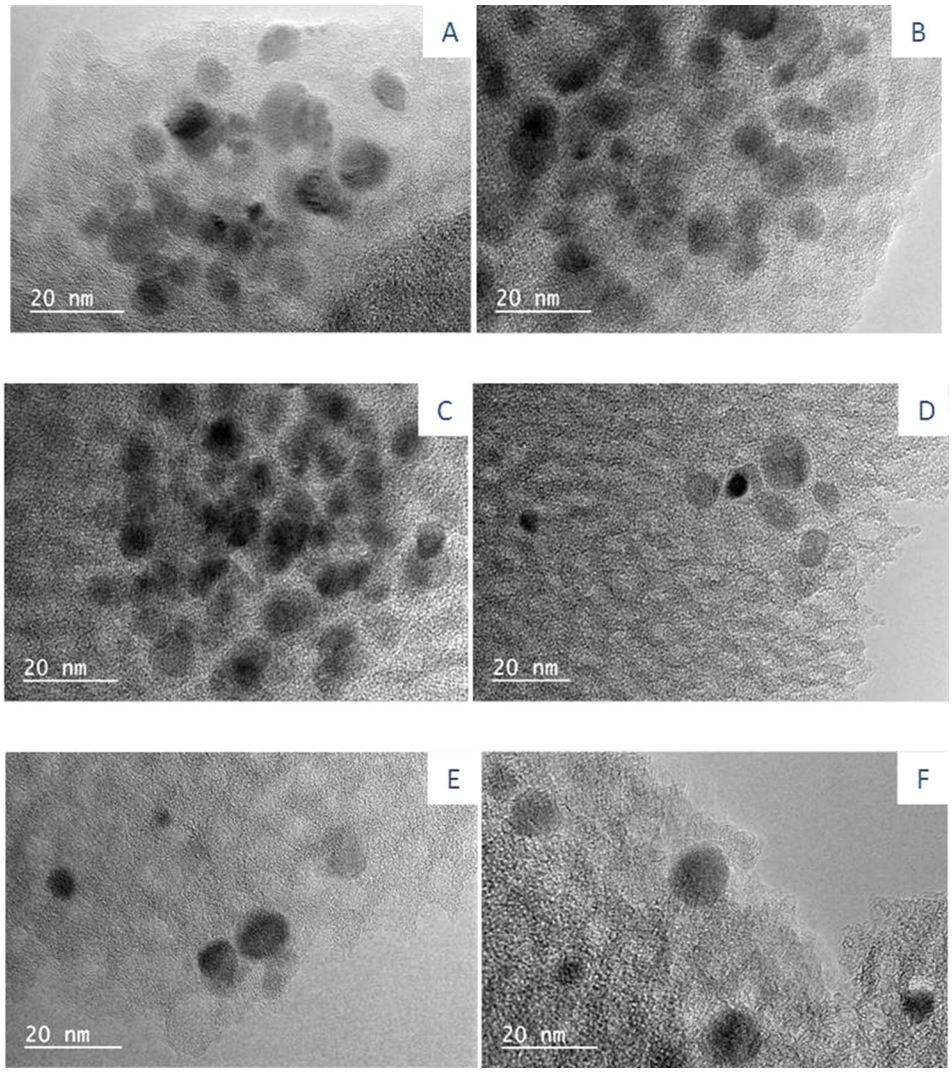

FIG. 3. Bright field TEM images for Ni@C-x composites with $x = 773$ K (a), 798 K (b), 823 K (c), 848 K (d), 873 K (e), and 973 K (f).

TABLE I. Physicochemical and magnetic properties of Ni@C-*x* composites ($x = 773$, 798, 823, 848, 873, and 973 K): the maximum combustion temperature of carbon by TGA experiments under air (T_{comb}), the Ni amount (wt. % over the entire composite mass) as determined by TGA experiments, the average particle size (nm) as obtained by TEM, and the saturation magnetization (M_S) at 300 K expressed as both emu over the entire mass of composite and emu over the mass of Ni.

Sample	T_{comb} by TGA (K)	Ni amount (wt. %)	Particle size by TEM (nm)	M_S at 300 K (emu/$g_{composite}$)	M_S at 300 K (emu/g_{Ni})
Ni@C-773	658	5.7	5.2	0.92(1)	16.1(1)
Ni@C-798	719	5.3	6.2	1.00(1)	18.8(1)
Ni@C-823	738	5.4	5.7	1.07(1)	19.8(1)
Ni@C-848	771	4.6	5.9	1.13(1)	24.5(1)
Ni@C-873	743	4.8	8.9	1.48(1)	30.8(1)
Ni@C-973	822	4.7	12.4	1.45(1)	30.8(1)

increases with the thermal annealing temperature. Two main factors may be responsible for the observed tendency: the first one is related to the increase in the particle size which decreases the catalytic effect of the Ni particles to burn the carbon[39,42] and the second one is assigned to an increase of the degree of graphitization of the carbon matrix.[43] Overall, the carbon is amorphous, as proven by XRD but also shows well graphitic domains around the Ni particles, as demonstrated by HR-TEM (Fig. SI-4, supplementary material).

B. Magnetic properties of one-pot Ni@C-*x* composites

From the physicochemical characterizations, Ni nanoparticles are metallic, as proven by XRD with the lattice parameter slightly larger than pure Ni. A small carbon amount dissolved in Ni nanoparticles might explain this small lattice expansion. The presence of C within Ni nanoparticles is expected by one-pot synthetic methods due to the simultaneous presence and intimate mixing of both carbon and metal precursors at the beginning of the annealing step, responsible for both carbonization of the carbon precursor and reduction of the metal salt. To assess the C amount in the Ni nanoparticles as a function of synthetic temperature, a

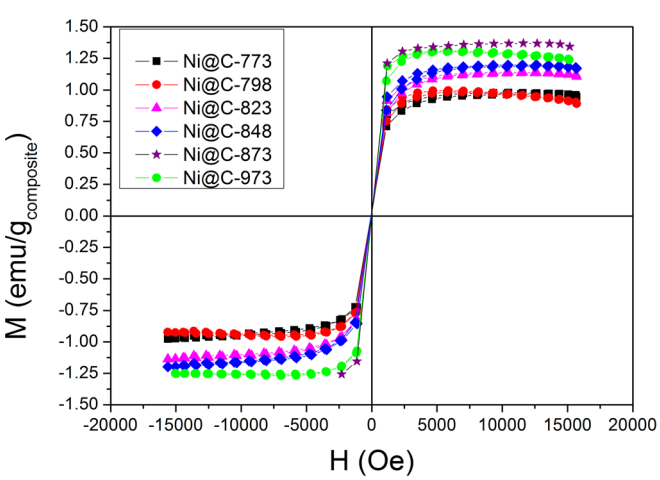

FIG. 4. Magnetization curves recorded at 300 K for all Ni@C-*x* composites ($x = 773$, 798, 823, 848, 873, and 973 K).

comparative study between experimental magnetization of Ni@C-*x* composites and theoretical modeling of Ni-C system was undertaken.

Ni nanoparticles with similar sizes (~5–20 nm) show superparamagnetic behavior at a low temperature with the blocking temperature around 100 K and the irreversible temperature between 150 and 180 K.[3,14] Consequently, in order to avoid the superparamagnetic domain that might introduce inaccuracy in the reading of the M_S values, we have chosen to perform the magnetic measurements at room temperature. This makes our proposed method fast and easy to implement since cryogenic temperatures, commonly used in magnetism, are no longer essential.

Magnetization curves, recorded at 300 K for all Ni@C-*x* composites, are displayed in Fig. 4 and the calculated M_S values are listed in Table I.

Generally, the saturation magnetization increases with the annealing temperature as expressed by both the mass of composite and the mass of Ni (Table I). However, these values are much lower than pure bulk Ni properties ($M_S = 53$ emu/g_{Ni} at 300 K). This trend can be related to two parameters: (i) the C concentration in Ni and (ii) size effects in Ni nanoparticles. Both factors can strongly influence the magnetic properties of Ni, as already reported.[1–4,44] First, a small amount of C in Ni reduces the magnetization compared to pure bulk Ni.[33] Moreover, for the highest C content in bulk Ni (25 at. %), i.e., nickel carbide Ni_3C, magnetism is completely suppressed.[45] This alloy is not ferromagnetic due to strong Ni-C hybridization. Second, it was experimentally observed that the decrease of the nanoparticle size reduces the M_S as compared to the bulk counterpart.[46] One suggested explanation is the inevitable formation of oxide layers (such as, antiferromagnetic NiO) at the surface of Ni nanoparticles. Smaller nanoparticles have higher surface-to-volume ratios consequently, the surface oxide layer is increasingly important with downsizing. Thus, M_S continuously decreases with the reducing size. Recently, Ishizaki *et al.* proposed a simple model to quantitatively assess the drop of M_S by reducing the nanoparticle size based on the assumption that only core Ni atoms contribute to the M_S whereas, the surface atoms are oxidized, thus being antiferromagnetic.[46] We have performed these calculations in the case of our Ni nanoparticles to account for the size effect (Fig. SI-5, supplementary material). As expected, the calculated M_S decreases from 48 to 40 emu/g_{Ni} whereas, we experimentally observed a change from 31 to 16 emu/g_{Ni} with the reducing size. The drop of M_S is more significant in our Ni nanoparticles and the magnetization range is very different relative to the calculated M_S. Therefore, the size effect cannot be solely invoked to explain the strong drop of M_S observed in our nanoparticles.

In the present case, the one-pot method allows the preparation of Ni nanoparticles well embedded within the carbon matrix, as we recently demonstrated for Co and Pd-Pt bimetallic nanoparticles synthesized by a similar one-pot route.[15,39] Indeed, the latter metallic nanoparticles are effectively confined in the carbon matrix and a graphite layer surrounds these particles. This confinement was clearly proven by using absorption measurements of the smallest probe molecule, i.e., hydrogen. Highly confined nanoparticles do not absorb hydrogen due to the graphitic surface layer that

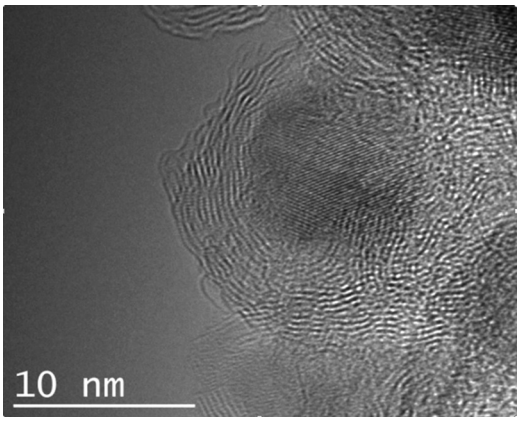

FIG. 5. HR-TEM image of a Ni nanoparticle of Ni@C-798 surrounded by a graphitic layer.

forbids the access of hydrogen to the particles. Similarly, the present Ni nanoparticles are confined within a graphite layer, as shown in the HR-TEM image in Fig. 5 (Ni@C-798). The formation of such a protective graphite layer was observed for all Ni@C-x composites, irrespective of the annealing temperature (Fig. SI-4, supplementary material). As a consequence, the present Ni nanoparticles are all surrounded by graphite and thus protected from oxidation upon air exposure. This also discards the second attempt to explain the reduction of M_S by surface oxidation with formation of the antiferromagnetic NiO layer. Moreover, the carbon confinement of Ni favors the first hypothesis to understand the drop of M_S by the presence of a small C concentration within Ni nanoparticles, as also suggested by the small increase of the *fcc* lattice parameter.

Ni is a well known catalyst for the growth of carbon nanotubes (CNTs) and graphitization of carbon materials. For the synthesis of CNTs, nanometer-size metal particles are required to enable hydrocarbon decomposition at a temperature lower than the spontaneous decomposition temperature of the hydrocarbon. The most commonly used metals are Fe, Co, and Ni, because of two main reasons: (i) high solubility of C in these metals and (ii) high C diffusion rate in these metals. Several steps are widely accepted to explain the growth of CNTs catalyzed by Ni nanoparticles: first, hydrocarbon vapor flow (carbon precursors) comes in contact with the metal nanoparticles and decomposes into carbon and hydrogen species; second, the gaseous hydrogen is removed by the continuous flow and carbon gets dissolved into the metal. After reaching the C solubility limit in the Ni metal at that temperature, the as dissolved C precipitates out and nucleates a C cap at the top of the catalyst; it then grows into a carbon nanotube. A similar growth mechanism may also occur during one-pot synthesis and can explain the encapsulation of Ni nanoparticles with a graphite layer. As the carbon precursor is in excess relative to the Ni amount, formation of graphitic carbon is limited to the neighboring of Ni nanoparticles, whereas the overwhelming rest of the carbon is formed in an amorphous state. The small amount of graphite around Ni is not noticeable by XRD contrary to TEM imaging that confirms graphite layers developed around Ni nanoparticles.

In this context, it becomes obvious that the drop of M_S in Ni@C-x composites can be related to the presence of C in Ni. However, we do not have a precise experimental method to determine the C content in Ni nanoparticles. Commonly used techniques such as, TEM-EDX, XPS etc., cannot inform about the accurate C amount in Ni since these nanoparticles are embedded into a carbon matrix.

An elegant way to overcome this difficulty is to perform Monte Carlo simulations and to calculate the magnetization of Ni nanoparticles for a wide range of C solubility (0–25 at. %). The size of nanoparticles was fixed to 10 nm in order to neglect possible size effect on the magnetization. First, the magnetization of the bulk *fcc* Ni-C system was calculated. Figure 6(a) shows the magnetic moments of Ni that decrease with the C concentration and are quenched for $x_c = 25\%$. Such tendency has already been observed by Fang *et al.*[28] It is well known that the local magnetic moment and the corresponding atomic volume, as well as the chemical environment, are directly correlated. As a result, the local magnetic moment tends to decrease with increasing coordination or

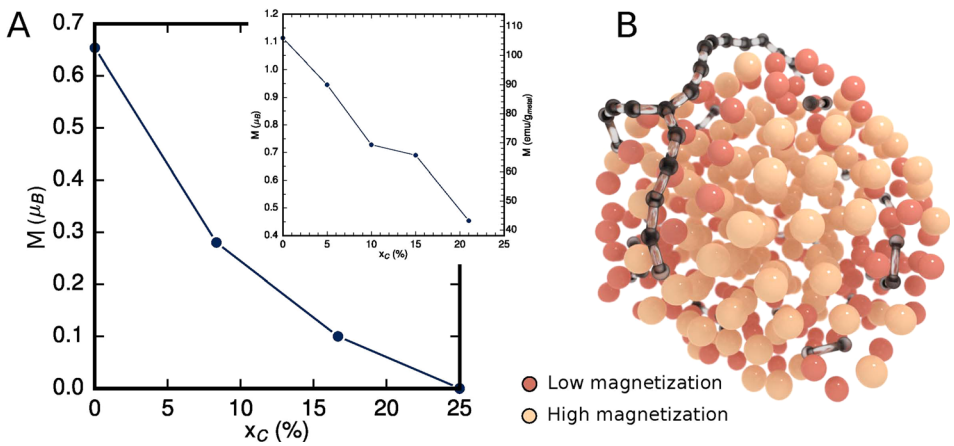

FIG. 6. (a) Magnetization of bulk Ni-C as a function of C concentration (at.%). The inset corresponds to the magnetization of Ni-C NP with 1.2 nm diameter as a function of the C concentration calculated by the DFT. (b) Snapshot of a Ni-C nanoparticle with 201 Ni atoms and 17 at. % C with both carbon atoms dissolved inside the nanoparticle and carbon adsorbed at the surface. This equilibrium configuration has been obtained after performing Grand Canonical Monte Carlo simulations at 1400 K and cooling down to 300 K. As a result, a part of carbon atoms segregate to the surface and self-organize to form chains at the surface of the nanoparticle.

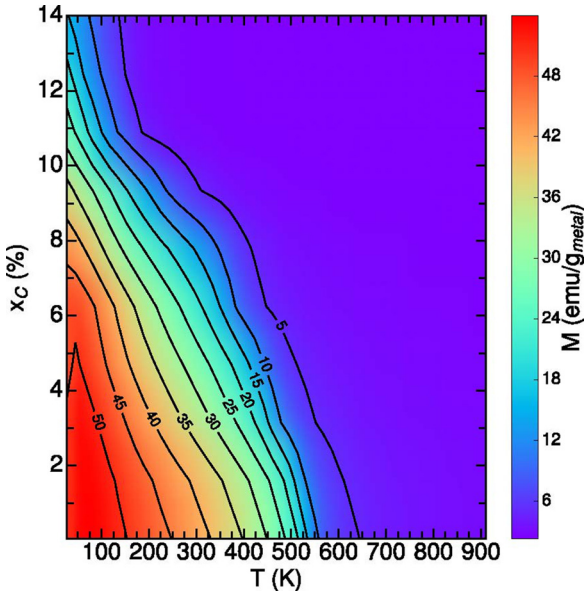

FIG. 7. Magnetization (emu/g_{metal}) isocurves as a function of temperature and carbon concentration within Ni as calculated by Monte Carlo simulations.

decreasing interatomic distance. This is typically the case in the present situation, where the calculations of the local magnetic moment of Ni as a function of C concentration are depicted. This, therefore, indicates that the presence of C atoms inside Ni leads to a reduced magnetization.

Second, we considered a disordered NP containing 201 Ni atoms and 40 C atoms [Fig. 6(b)]. This equilibrium configuration has been obtained by performing GCMC calculations, starting from a pure Ni NP, with a temperature and a C chemical potential, relevant to calculate a point in the phase diagram of Ni-C NPs.[10] Then, local magnetic moments of this C-enriched NP are investigated by performing DFT calculations. It should be noted that all atomic coordinates are kept fixed because a complete relaxation is hardly feasible. Nevertheless, this limitation does not prevent us to describe qualitatively the magnetic properties of NPs containing C atoms. Different populations of Ni atoms can be identified. First, Ni atoms close to the surface have a high magnetic moment (around 1.1 μ_B). As the number of C neighbors around a Ni atom decreases, its magnetic moment is increased. This simple rule can be applied to explain the modified magnetism of Ni atoms in the presence of C atoms as the first neighbors.

Figure 7 displays the magnetization isocurves as a function of temperature and carbon concentration in Ni nanoparticles (x_C) obtained by Monte Carlo modeling. Thus, we can easily determine the C solubility from the values of M_S expressed as emu/g_{Ni} (Table I).

The variations of the C concentration values (x_C) together with M_S versus thermal treatment temperature during one-pot synthesis are shown in Fig. 8.

It becomes obvious that Ni nanoparticles prepared by the present one-pot synthetic method contain a significant amount of C and the latter value decreases from around 8 to 4 at. % by increasing the treatment temperature from 773 to 997 K. In this temperature range, the solubility of C in the bulk Ni metal is comprised between 2 and 8 at. %, which is

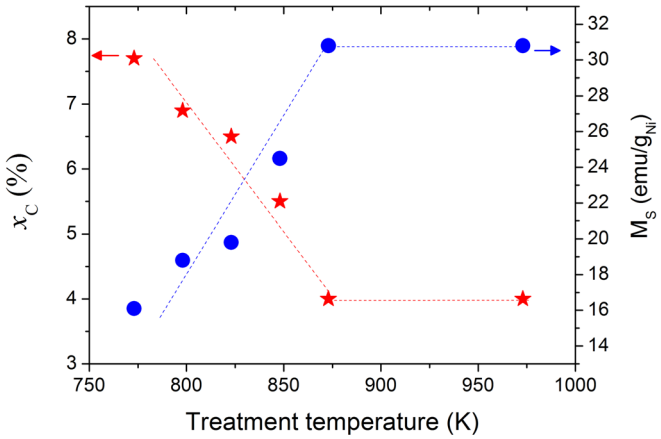

FIG. 8. The evolution of M_S (blue circles) of Ni@C-x composites and the estimated C content (red stars) in Ni nanoparticles with treatment temperature during one-pot synthesis. The dotted lines are a guide to the eye.

in very good agreement with our data.[47] However, the trend in our nanoparticles is in disagreement with the enhancement of the C concentration in bulk Ni with the rising temperature.[47] Moreover, the C concentration in Ni nanoparticles reaches a stable value of around 4 at. % at 873 K and a further increase of temperature to 973 K does not have any influence on the carbon content. The one-pot synthetic process might be responsible for this apparent contradictory thermal behavior. A possible hypothesis is based on the nucleation and growth of Ni-based nanoparticles from the initial mixture of carbon and Ni precursors with soft-template agents. Ni nanoparticles containing a large amount of dissolved C first nucleate and grow within the surrounding matrix. Early graphite layers are also formed at the surface of nanoparticles by a dissolution-precipitation mechanism due to the catalytic properties of Ni to decompose the carbon precursor at low temperature. This graphite layer around Ni might block further dissolution of carbon in Ni from the outside carbon source. Thus, increasing the thermal treatment temperature increases the thickness of the graphite layer at the surface by the depletion of the C content in Ni nanoparticles.[23] The increase of the amount of graphitic layer is in good agreement with TGA combustion analysis.

Thus, tuning the thermal conditions of the one-pot method allows the control of the C content in magnetic Ni nanoparticles. Moreover, these nanoparticles are covered with a graphite layer that acts as a protective barrier from oxidation upon air exposure.

IV. CONCLUSIONS

In summary, we propose an elegant combination between experimental results based on magnetization at room temperature and Monte Carlo simulations to track the C content within Ni nanoparticles embedded in the carbon matrix. Thermal treatments are key for tailoring the C content in Ni nanoparticles synthesized by the one-pot route: higher process temperature and lower carbon solubility in Ni nanoparticles. The choice of magnetic measurements at room temperature makes our proposed method fast and easy

to implement since cryogenic temperatures, commonly used in magnetism, are no longer essential.

SUPPLEMENTARY MATERIAL

See supplementary material for Figure SI-1. Raman spectra for all Ni@C-x composites with $x = 773$ K, 798 K, 823 K, 848 K, 87 K, and 973 K. Figure SI-2. Particles size histograms for all Ni@C-x composites with $x = 773$ K (A), 798 K (B), 823 K (C), 848 K (D), 873 K (E) and 973 K (F). Figure SI-3. TGA curves under air and related derivatives for all Ni@C-x composites. Figure SI-4. TEM images of Ni@C-798 (left) and Ni@C-823 (right) composites showing graphite layers developed around Ni nanoparticles. Figure SI-5. The comparison between Ms measured and calculated following the equation proposed by Ishizaki *et al.*[1]

ACKNOWLEDGMENTS

The authors acknowledge the French National Research Agency (ANR) for the financial support under GENESIS Contract No. 13-BS08-0004. G. Schrodj and L. Vidal are acknowledged for performing TGA and TEM analyses through the IS2M technical platform. Y. Magnin gratefully acknowledges the UCP, Computational Center of the Cergy-Pontoise University for the CPU time used to perform numerical simulations.

[1]J.-H. Hwang, V. P. Dravid, M. H. Teng, J. J. Host, B. R. Elliott, D. L. Johnson, and T. O. Mason, J. Mater. Res. **12**, 1076 (1997).
[2]X.-C. Sun and X.-L. Dong, Mater. Res. Bull. **37**, 991 (2002).
[3]R. Campesi, V. Paul-Boncour, F. Cuevas, E. Leroy, R. Gadiou, C. Vix-Guterl, and M. Latroche, J. Phys. Chem. C **113**, 16921 (2009).
[4]H. T. Zhang, G. Wu, X. H. Chen, and X. G. Qiu, Mater. Res. Bull. **41**, 495 (2006).
[5]J. Kudrnovský, V. Drchal, and P. Bruno, Phys. Rev. B **77**, 224422 (2008).
[6]M. Kumar, in *Carbon Nanotubes–Synthesis Characterisation Application*, edited by S. Yellampalli (InTech, Rijeka, 2011).
[7]C. P. Deck and K. Vecchio, Carbon **44**, 267 (2006).
[8]J. Robertson, J. Mater. Chem. **22**, 19858 (2012).
[9]V. K. Portnoi, A. V. Leonov, S. N. Mudretsova, and S. A. Fedotov, Phys. Met. Metallogr. **109**, 153 (2010).
[10]Y. Magnin, A. Zappelli, H. Amara, F. Ducastelle, and C. Bichara, Phys. Rev. Lett. **115**, 205502 (2015).
[11]M. He, Y. Magnin, H. Amara, H. Jiang, H. Cui, F. Fossard, A. Castan, E. Kauppinen, A. Loiseau, and C. Bichara, Carbon **113**, 231 (2017).
[12]J.-M. Aguiar-Hualde, Y. Magnin, H. Amara, and C. Bichara, Carbon **120**, 226 (2017).
[13]Y. Zhai, Y. Dou, X. Liu, B. Tu, and D. Zhao, J. Mater. Chem. **19**, 3292 (2009).
[14]A. Martínez de Yuso, J.-M. Le Meins, Y. Oumellal, V. Paul-Boncour, C. Zlotea, and C. M. Ghimbeu, J. Nanopart. Res. **18**, 380 (2016).
[15]A. Martinez de Yuso, Y. Oumellal, C. Zlotea, L. Vidal, and C. M. Ghimbeu, Nano-Struct. Nano-Objects **9**, 1 (2017).
[16]C. M. Ghimbeu, A. Puscasu, A. M. de Yuso, C. Zlotea, Y. Oumellal, M. Latroche, and C. Vix-Guterl, Microporous Mesoporous Mater. **223**, 79 (2016).
[17]C. M. Ghimbeu, J.-M. L. Meins, C. Zlotea, L. Vidal, G. Schrodj, M. Latroche, and C. Vix-Guterl, Carbon **67**, 260 (2014).
[18]J. Hoekstra, A. M. Beale, F. Soulimani, M. Versluijs-Helder, J. W. Geus, and L. W. Jenneskens, J. Phys. Chem. C **119**, 10653 (2015).
[19]W. Weisweiler, N. Subramanian, and B. Terwiesch, Carbon **9**, 755 (1971).
[20]A. Ōya and H. Marsh, J. Mater. Sci. **17**, 309 (1982).
[21]C. Bellouard, G. Mercier, S. Cahen, J. Ghanbaja, G. Medjahdi, J. Gleize, G. Lamura, C. Hérold, and B. Vigolo, J. Magn. Magn. Mater. **411**, 39 (2016).
[22]H. Amara, J.-M. Roussel, C. Bichara, J.-P. Gaspard, and F. Ducastelle, Phys. Rev. B **79**, 014109 (2009).
[23]R. S. Weatherup, H. Amara, R. Blume, B. Dlubak, B. C. Bayer, M. Diarra, M. Bahri, A. Cabrero-Vilatela, S. Caneva, P. R. Kidambi, M.-B. Martin, C. Deranlot, P. Seneor, R. Schloegl, F. Ducastelle, C. Bichara, and S. Hofmann, J. Am. Chem. Soc. **136**, 13698 (2014).
[24]M. Diarra, A. Zappelli, H. Amara, F. Ducastelle, and C. Bichara, Phys. Rev. Lett. **109**, 185501 (2012).
[25]M. Mrovec, D. Nguyen-Manh, C. Elsässer, and P. Gumbsch, Phys. Rev. Lett. **106**, 246402 (2011).
[26]D. W. Boukhvalov, Y. N. Gornostyrev, M. I. Katsnelson, and A. I. Lichtenstein, Phys. Rev. Lett. **99**, 247205 (2007).
[27]S. Karoui, H. Amara, B. Legrand, and F. Ducastelle, J. Phys. Condens. Matter **25**, 056005 (2013).
[28]C. M. Fang, M. H. F. Sluiter, M. A. van Huis, and H. W. Zandbergen, Phys. Rev. B **86**, 134114 (2012).
[29]P. Yu, X. F. Jin, J. Kudrnovský, D. S. Wang, and P. Bruno, Phys. Rev. B **77**, 054431 (2008).
[30]D. J. Siegel, M. van Schilfgaarde, and J. C. Hamilton, Phys. Rev. Lett. **92**, 086101 (2004).
[31]F. C. Schwerer, J. Appl. Phys. **40**, 2705 (1969).
[32]A. Cottrell, *Chemical Bonding in Transition Metal Carbides* (The Institute of Materials, London, 1995).
[33]D. J. Siegel and J. C. Hamilton, Phys. Rev. B **68**, 094105 (2003).
[34]P. Giannozzi, S. Baroni, N. Bonini, M. Calandra, R. Car, C. Cavazzoni, D. Ceresoli, G. L. Chiarotti, M. Cococcioni, I. Dabo, A. Dal Corso, S. de Gironcoli, S. Fabris, G. Fratesi, R. Gebauer, U. Gerstmann, C. Gougoussis, A. Kokalj, M. Lazzeri, L. Martin-Samos, N. Marzari, F. Mauri, R. Mazzarello, S. Paolini, A. Pasquarello, L. Paulatto, C. Sbraccia, S. Scandolo, G. Sclauzero, A. P. Seitsonen, A. Smogunov, P. Umari, and R. M. Wentzcovitch, J. Phys. Condens. Matter **21**, 395502 (2009).
[35]P. E. Blöchl, Phys. Rev. B **50**, 17953 (1994).
[36]J. P. Perdew, K. Burke, and M. Ernzerhof, Phys. Rev. Lett. **77**, 3865 (1996).
[37]I. R. Shein, N. I. Medvedeva, and A. L. Ivanovskii, Phys. Rev. B: Condens. Matter **371**, 126 (2006).
[38]X. Hu, T. Björkman, H. Lipsanen, L. Sun, and A. V. Krasheninnikov, J. Phys. Chem. Lett. **6**, 3263 (2015).
[39]C. M. Ghimbeu, M. Sopronyi, F. Sima, L. Delmotte, C. Vaulot, C. Zlotea, V. Paul-Boncour, and J.-M. Le Meins, Nanoscale **7**, 10111 (2015).
[40]C. Pardanaud, C. Martin, P. Roubin, G. Giacometti, C. Hopf, T. Schwarz-Selinger, and W. Jacob, Diamond Relat. Mater. **34**, 100 (2013).
[41]C. Zlotea, C. M. Ghimbeu, Y. Oumellal, J.-C. Crivello, C. Vix-Guterl, and M. Latroche, Nanoscale **7**, 15469 (2015).
[42]P. Dibandjo, C. Zlotea, R. Gadiou, C. M. Ghimbeu, F. Cuevas, M. Latroche, E. Leroy, and C. Vix-Guterl, Int. J. Hydrogen Energy **38**, 952 (2013).
[43]M. Sevilla and A. B. Fuertes, Carbon **56**, 155 (2013).
[44]W. H. Zhong, C. Q. Sun, and S. Li, Solid State Commun. **130**, 603 (2004).
[45]L. Yue, R. Sabiryanov, E. M. Kirkpatrick, and D. L. Leslie-Pelecky, Phys. Rev. B **62**, 8969 (2000).
[46]T. Ishizaki, K. Yatsugi, and K. Akedo, Nanomaterials **6**, 172 (2016).
[47]J. J. Lander, H. E. Kern, and A. L. Beach, J. Appl. Phys. **23**, 1305 (1952).